Pion double charge exchange on $T=1$ nuclei

Peter A. Seidl, Mark D. Brown, Rex R. Kiziah, and C. Fred Moore
University of Texas at Austin, Austin, Texas 78712

Helmut Baer and C. L. Morris
Los Alamos National Laboratory, Los Alamos, New Mexico 87545

G. R. Burleson, W. B. Cottingame, and Steven J. Greene*
New Mexico State University, Las Cruces, New Mexico 88003

L. C. Bland† and R. Gilman
University of Pennsylvania, Philadelphia, Pennsylvania 19104

H. T. Fortune‡
Los Alamos National Laboratory, Los Alamos, New Mexico 87545
and University of Pennsylvania, Philadelphia, Pennsylvania 19104
(Received 9 January 1984)

New measurements of $^{14}C,^{26}Mg(\pi^+,\pi^-)$ differential cross sections are reported and compared to previous differential cross sections for double charge exchange on $T \geq 1$ nuclei.

I. INTRODUCTION

To date, measurements of the small-angle excitation function of (π^+,π^-) double-charge-exchange (DCX) reactions on $T \geq 1$ target nuclei have been reported for three cases—the $T=1$ nuclei ^{18}O and ^{26}Mg (Ref. 1), and the $T=2$ nucleus ^{56}Fe.[2] In all three instances (see Fig. 1) the data for the DCX process leading to the double-isobaric-analog state (DIAS)—the ground state in ^{18}Ne and ^{26}Si and the 0^+, $T=2$ state at 9.6 MeV in ^{56}Ni—exhibit a rapidly varying cross section as a function of pion energy.[1,2] For ^{18}O and ^{26}Mg, the energy dependence is that of a peak 60—80 MeV wide centered near 140 MeV and a monotonic increase of the cross section between 200 and 300 MeV.

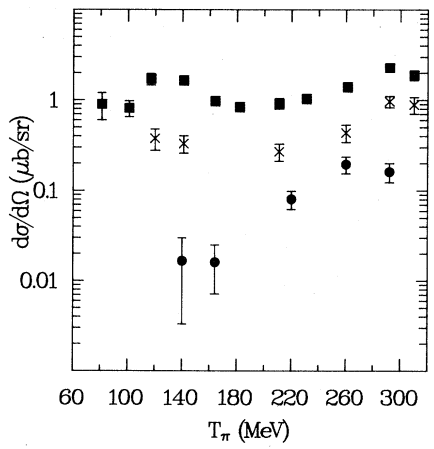

FIG. 1. Excitation functions measured at $\theta_{lab}=5°$ for $^{18}O(\pi^+,\pi^-)^{18}Ne$(DIAS) (squares) and $^{26}Mg(\pi^+,\pi^-)^{26}Si$(DIAS) (crosses) from Ref. 1, and $(d\sigma/d\Omega)/2$ for $^{56}Fe(\pi^+,\pi^-)^{56}Ni$(DIAS, 9.6 MeV) (circles) from Ref. 2.

For ^{56}Fe, the cross section shows only the second feature. At $T_\pi=292$ MeV, angular distributions for $^{18}O(\pi^+,\pi^-)^{18}Ne$(DIAS) and $^{26}Mg(\pi^+\pi^-)^{26}Si$(DIAS) exhibit diffractive shapes with first minima at momentum transfers consistent with the nuclear sizes. However, at $T_\pi=164$ MeV the $^{18}O(\pi^+,\pi^-)^{18}Ne$(DIAS) angular distribution has a minimum at $\theta=20°$, corresponding to an unphysically large radius. The occurrence of a minimum at a small scattering angle is not explained by any simple[3,4] two-step pion-nucleus calculation. Prior to the present work, there was no $T_\pi=164$ MeV angular distribution for $^{26}Mg(\pi^+,\pi^-)^{26}Si$(DIAS).

Experimental data have shown the dependence of the forward-angle cross section on target mass to be roughly $A^{-10/3}$ (Ref. 2), in agreement with the geometric model of Johnson,[3] which assumes that the reaction proceeds in two steps via a matrix element proportional to A^{-1}. For $A=18$, the cross section at $\theta_{lab}=5°$ and at energies near the peak of the π-nucleon $\Delta_{3/2,3/2}(1232)$ resonance is about 1 μb/sr.

In contrast, DCX on $T=0$ nuclei (which, of necessity, must be nonanalog in character) have exhibited peaked excitation functions with a centroid and width of about 160 and 70 MeV, respectively.[5] The forward-angle cross section is about 0.5 μb for $A=16$ near the maximum of the excitation function and the target mass dependence[6] is roughly $A^{-4/3}$.

Almost all theoretical DCX work has concentrated on analog transitions.[7,8] Liu[7] uses a coupled-channels optical potential and includes sequential one-nucleon single-charge-exchange (SCX) processes, with terms proportional to ρ^2 in the potential. True pion absorption and scattering of a pion by two short-range correlated nucleons are the reaction mechanisms considered in the calculation of the ρ^2 terms, though the latter process is estimated to be

unimportant at energies below $T_\pi = 180$ MeV. In Ref. 7, calculations are compared to the measured angular distributions and the excitation function for $^{18}O(\pi^+,\pi^-)^{18}Ne$(DIAS). For these calculations, the effects of core excitation were found to be important.

The theoretical work of Johnson and Siciliano[8] is also based on a coupled-channels optical potential and includes terms proportional to ρ^2. The theory is constructed in an isospin invariant framework. The parameters of the first order potential are determined by the free pion-nucleon phase shifts. The elastic, SCX, and DCX amplitudes are obtained by taking linear combinations of the pion-nucleus scattering amplitudes on channels of total isospin (nuclear plus pion). The Coulomb interaction is not included in their theory. Their second-order potential is constructed with the purpose of obtaining a set of phenomenological parameters to describe elastic scattering, SCX, and DCX reactions from a given nucleus at a given energy. Most of these parameters are weakly dependent on target mass, but are strongly energy dependent. DCX reactions that lead to double isobaric analog states are currently being explored in terms of the isobaric multiplet approach of Johnson and Siciliano.[8] A systematic analysis of elastic scattering, single charge exchange, and double charge exchange leading to analog states is underway.[9] The new $^{14}C(\pi^+,\pi^-)$ measurements reported herein are part of a study of pion elastic scattering,[10] SCX, and DCX reactions on a single $T=1$ isotope.

In this paper we present new angular distributions for $^{14}C,^{26}Mg(\pi^+,\pi^-)^{14}O,^{26}Si$(DIAS) at $T_\pi = 164$ MeV, $^{14}C(\pi^+,\pi^-)^{14}O$(DIAS) at $T_\pi = 292$ MeV, a 5° excitation function ($120 \leq T_\pi \leq 292$ MeV) for

$$^{14}C(\pi^+,\pi^-)^{14}O(\text{DIAS}),$$

and forward angle ($\theta_{lab} = 5°$) differential cross sections at $T_\pi = 120$, 164, and 180 MeV for

$$^{26}Mg(\pi^+,\pi^-)^{26}Mg(\text{DIAS}).$$

In addition, a 5° excitation function and an angular distribution at $T_\pi = 164$ MeV were extracted for the reaction $^{14}C(\pi^+,\pi^-)^{14}O(E_x \simeq 5.9$ MeV).

II. EXPERIMENT

This experiment was performed at the Energetic Pion Channel and Spectrometer (EPICS) at the Clinton P. Anderson Meson Physics Facility (LAMPF). The standard EPICS system and DCX modifications have been described in detail elsewhere.[11] The pion beam spot size on target is about 8 cm ×20 cm. The dispersed beam technique, in which pion position at the target is correlated with momentum, allows the momentum of the scattered pion to be determined with much better accuracy than the momentum acceptance of the beam ($\Delta p/p = \pm 1\%$). Table I shows that the range of Q values involved does not exceed the useful acceptance range of the spectrometer ($\Delta p/p = 14\%$). By using a composite target and ray tracing the trajectory of the scattered pion back from the focal plane of the spectrometer to the target, one can obtain data on two or more target species simultaneously. A summary of the target properties is given in Table II, and a schematic of the arrangement of these targets in the scattering chamber is shown in Fig. 2. Missing mass spectra for $^{14}C(\pi^+,\pi^-)$ and $^{26}Mg(\pi^+,\pi^-)$ are shown in Fig. 3. The peaks for the DIAS are well separated in energy from the other low-lying states (Fig. 4) of the residual nuclei ^{14}O and ^{26}Si.

Normalizations of the DCX cross sections were obtained by measuring relative yields for $^1H(\pi^+,\pi^+)^1H$ for all incident beam energies at a laboratory angle of 50° with a CH_2 target of areal density 73.5 mg/cm^2. Absolute normalization factors were determined by comparing these yields to cross sections calculated from the π-p phase-shift fits of Rowe, Salomon, and Landau.[12] The overall normalization is accurate to ±10%.

TABLE I. Nuclear g.s. Q values for double-charge-exchange reactions.

Reaction	Q value (MeV)
$^{13}C(\pi^+,\pi^-)^{13}O$	−18.959±0.013
$^{14}C(\pi^+,\pi^-)^{14}O$(DIAS)	−3.967±0.009
$^{26}Mg(\pi^+,\pi^-)^{26}Si$(DIAS)	−8.045±0.011
$^{56}Fe(\pi^+,\pi^-)^{56}Ni$	−5.679±0.014

TABLE II. Target properties.

Target isotope	Chemical composition	Isotopic purity (%)	Isotopic thickness (g/cm^2)	Dimensions (cm)
^{13}C	C	90	1.340	9.2×10.0[a]
			0.635	10.2×11.3[b]
^{14}C	C	80	0.144	5. ×10.
^{26}Mg	Mg	100	0.815	7.5× 8.0
^{56}Fe	carbon steel	90.1	2.3	5.8×12.7[c]
				9. ×12.7[d]
^1H	CH_2		0.0105	10. ×20.

[a]Configuration (a) and (c) of Fig. 2.
[b]Configuration (c) (top) of Fig. 2.
[c]Top of configuration (b) of Fig. 2.
[d]Bottom of configuration (b) of Fig. 2.

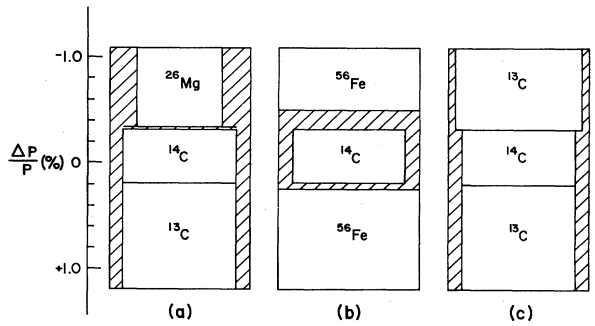

FIG. 2. Schematic of the target arrangement in the EPICS momentum dispersed pion beam. Data from the ^{13}C targets are presented in a companion paper [P. A. Seidl *et al.*, Phys. Rev. C **30**, 973 (1984)].

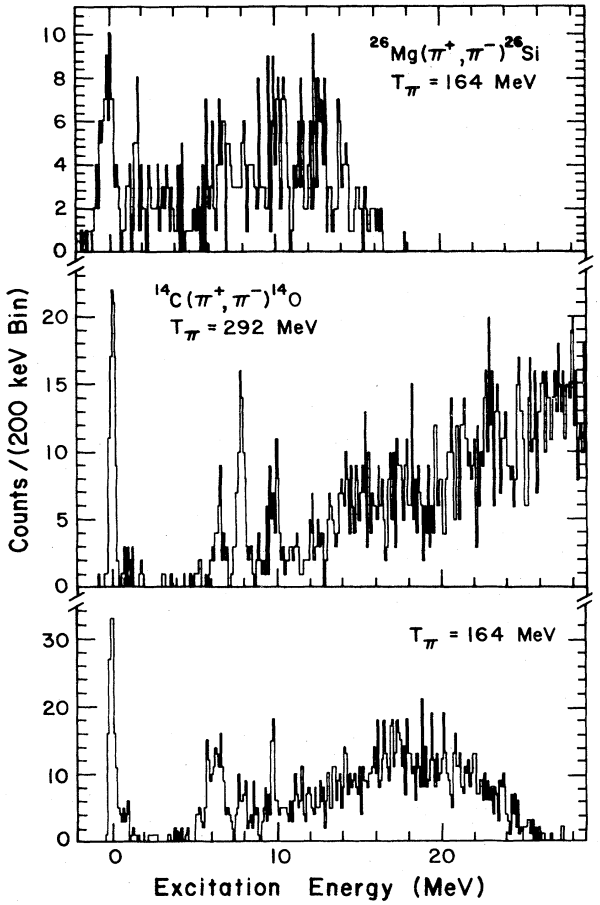

FIG. 3. Missing mass spectra of ^{26}Mg(π^+,π^-)^{26}Si (top) and ^{14}C(π^+,π^-)^{14}O (bottom) at $T_\pi=164$ and 292 MeV, summed over all angles for which data were taken. The spectra are not corrected for spectrometer acceptance as a function of outgoing pion momentum.

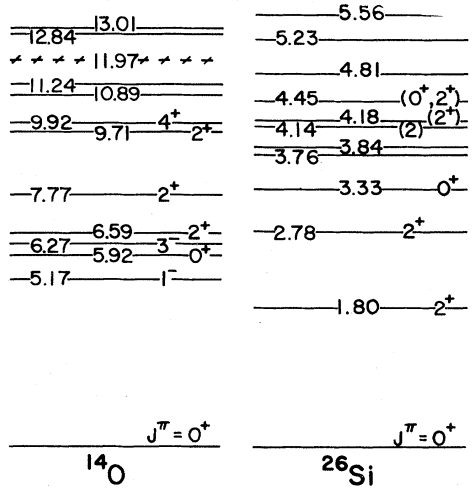

FIG. 4. Energy level diagrams of ^{14}O and ^{26}Si. Excitation energies are in units of MeV.

III. RESULTS

A. Excitation functions

The new data (see Tables III–V) are shown in Fig. 5, and compared with other[1] excitation functions for $T=1$ target nuclei in Fig. 6. The new datum for ^{26}Mg(π^+,π^-)^{26}Si(DIAS) at $T_\pi=120$ MeV agrees with the previous measurement,[1] and the new data at 164 and 180 MeV make clear the similarity of the excitation functions for ^{18}O and ^{26}Mg. Both are peaked at $T_\pi\simeq140$ MeV, have a minimum near $T_\pi\simeq170$ MeV, and increase towards the maximum measured energy of 292 MeV. The energy dependence[13] of ^{42}Ca(π^+,π^-)^{42}Ti(DIAS) is consistent with the above description for that of ^{18}O and ^{26}Mg. The statistical uncertainty of the ^{48}Ca(π^+,π^-)^{48}Ti(DIAS, $E_x=17.38$ MeV) and the ^{48}Ti(π^+,π^-)^{48}Cr(DIAS, $E_x=8.75$ MeV) excitation-function data[13] makes difficult the determination of the existence of a maximum near 140 MeV.

On the other hand, the excitation functions for ^{14}C(π^+,π^-)^{14}O(DIAS) and ^{56}Fe(π^+,π^-)^{56}Ni($E_x=9.6$ MeV, DIAS) (see Table VI) increase monotonically over the energy range measured, as shown in Fig. 5. The shapes of the excitation functions for ^{14}C and ^{56}Fe are in agreement with lowest-order optical potential calculations of Johnson and Siciliano, generated from the computer program PIESDEX.[8]

TABLE III. Center-of-mass cross sections for ^{14}C(π^+,π^-)^{14}O(DIAS).

$T_\pi=164$ MeV		$T_\pi=292$ MeV		$\theta_{lab}=5°$	
θ_{lab} (deg)	$d\sigma/d\Omega$ (μb/sr)	θ_{lab} (deg)	$d\sigma/d\Omega$ (μb/sr)	T_π (MeV)	$d\sigma/d\Omega$ (μb/sr)
0	1.29 ±0.27	0	4.28 ±0.74	120	0.903±0.242
5	1.00 ±0.10	5	4.25 ±0.55	140	0.807±0.151
10	0.841±0.141	10	2.28 ±0.42	164	1.00 ±0.10
15	0.779±0.151	14	1.49 ±0.32	180	1.82 ±0.29
17.5	0.223±0.074	23	0.399±0.123	220	2.72 ±0.32
20	0.216±0.065	27.5	0.030±0.030	260	4.08 ±0.52
25	0.136±0.045	32	0.021±0.021	292	4.25 ±0.55
33	0.195±0.058	41	0.108±0.054		
40	0.119±0.040	50	0.261±0.071		
50	0.131±0.049				

TABLE IV. Center-of-mass cross sections for $^{14}C(\pi^+,\pi^-)^{14}O(E_x\simeq 5.9$ MeV).

$T_\pi=164$ MeV		$\theta_{lab}=5°$	
θ_{lab} (deg)	$d\sigma/d\Omega$ (μb/sr)	T_π (MeV)	$d\sigma/d\Omega$ (μb/sr)
0	0.124±0.062	120	0.202±0.101
5	0.222±0.044	140	0.555±0.126
10	0.331±0.102	164	0.222±0.044
15	0.191±0.082	180	0.244±0.082
17.5	0.176±0.088	220	0.183±0.073
20	0.118±0.039	260	≤0.068
25	0.041±0.020	292	≤0.058
33	0.053±0.036		
40	0.091±0.036		
50	0.045±0.030		

The energies of the 0^+, 3^-, and 2^+ states of ^{14}O are 5.92, 6.27, and 6.59 MeV, respectively. The FWHM energy resolution for the spectrum is 400–500 keV, making reliable extraction of cross sections difficult for these states. The excitation function for a region 0.5 MeV wide centered about the position of the 0^+, 5.92 MeV state is shown in Fig. 7, along with that for the $^{56}Fe(\pi^+,\pi^-)^{56}Ni$(g.s.) reaction. Both decrease with increasing pion kinetic energy, a feature also seen in other $\Delta J=0$ nonanalog DCX reactions.[5] The data are compared with curves obtained from a Breit-Wigner expression for the cross section, plus a background proportional to the PIESDEX cross sections (Fig. 5) to account for the less dominant sequential reaction mechanism. In Ref. 5, Breit-Wigner expressions were used to extract peak positions and widths for the excitation functions on $T=0$ target nuclei. For the nonanalog transitions shown in Fig. 8 we have fixed the widths to be 70 MeV (an average value from Ref. 5) and have fitted the data to obtain peak positions of 148 and 149 MeV for $^{14}C(\pi^+,\pi^-)^{14}O(E_x\simeq 5.9$ MeV) and $^{56}Fe(\pi^+,\pi^-)^{56}Ni$(g.s.), respectively. These peak positions are 10–20 MeV lower than those reported for the reactions studied in Ref. 5.

TABLE V. Center-of-mass cross sections for $^{26}Mg(\pi^+,\pi^-)^{26}Si$(DIAS).

$T_\pi=164$ MeV		$\theta_{lab}=5°$	
θ_{lab} (deg)	$d\sigma/d\Omega$ (μb/sr)	T_π (MeV)	$d\sigma/d\Omega$ (μb/sr)
0	0.322±0.097	120	0.259±0.078
5	0.242±0.054	164	0.242±0.054
10	0.106±0.040	180	0.206±0.061
15	0.028±0.014		
17.5	≤0.018		
20	≤0.010		
25	0.086±0.032		
33	0.140±0.038		
40	0.164±0.039		
50	0.016±0.008		

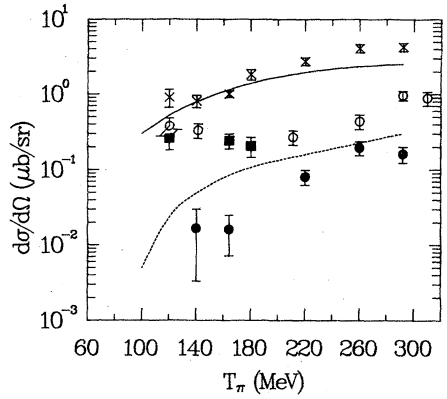

FIG. 5. New DIAS 5° excitation function data for $^{14}C(\pi^+,\pi^-)^{14}O$ (crosses) and $^{26}Mg(\pi^+,\pi^-)^{26}Si$ (squares for this work and open circles from Ref. 1). The closed circles are $(d\sigma/d\Omega)/2$ for $^{56}Fe(\pi^+,\pi^-)^{56}Ni$(DIAS, $E_x=9.6$ MeV) from Ref. 2. The solid and dashed curves are lowest-order PIESDEX (Ref. 7) calculations for $^{14}C(\pi^+,\pi^-)^{14}O$(DIAS) and $^{56}Fe(\pi^+,\pi^-)^{56}Ni$(DIAS, $E_x=9.6$ MeV), respectively.

B. Angular distributions

The new angular distributions for

$$^{14}C,^{26}Mg(\pi^+,\pi^-)^{14}O,^{26}Si(DIAS)$$

at $T_\pi=164$ MeV are compared with those for ^{18}O in Fig. 8. At $T_\pi=164$ MeV, the ^{18}O and ^{26}Mg angular distributions have first minima occurring at small momentum transfers. The $^{14}C(\pi^+,\pi^-)^{14}O$(DIAS) angular distribution does not possess a well-defined minimum, perhaps due to nuclear structure effects peculiar to ^{14}C. However, the decrease in cross section between 0° and 20° is consistent with a shallow minimum near $\theta\simeq 20°$. The ratios of the first maximum to the second maximum in the three angular distributions are a smooth function of A: 5.1±1.7, 4.0±0.9, and 1.5±0.5 for

$$^{14}C,^{18}O,^{26}Mg(\pi^+,\pi^-)^{14}O,^{18}Ne,^{26}Si(DIAS),$$

respectively.

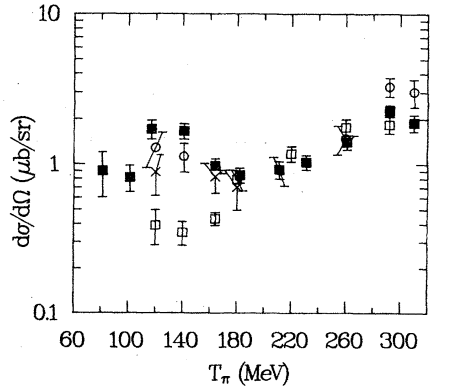

FIG. 6. DIAS excitation functions of $^{14}C(\pi^+,\pi^-)^{14}O$ (open squares), $^{18}O(\pi^+,\pi^-)^{18}Ne$ (solid squares, from Ref. 1), and $^{16}Mg(\pi^+,\pi^-)^{26}Si$ (crosses are new data, open circles are from Ref. 1). The data for ^{14}C and ^{26}Mg, multiplied by ratios of $A^{-10/3}$, are displayed on the scale of the ^{18}O data.

TABLE VI. Center-of-mass cross sections for ^{56}Fe(π^+,π^-)^{56}Ni at $\theta_{lab}=5°$.

T_π (MeV)	$d\sigma/d\Omega$ (μb/sr) DIAS, $E_x=9.6$ MeV	$d\sigma/d\Omega$ (μb/sr) g.s.
140	0.033±0.027	0.075±0.023
164	0.032±0.018	0.053±0.014
220	0.161±0.036	0.014±0.007
260	0.390±0.081	0.014±0.014
292	0.323±0.077	≤0.013

The three angular distributions at $T_\pi=292$ MeV (Fig. 8) are similar in that they exhibit deep minima at momentum transfers consistent with strong-absorption radii for those nuclei. Data are lacking in the region of the second maximum, making a comparison of the cross sections at the first and second maxima impossible at this energy.

Optical-potential calculations have been performed with the computer program PIESDEX (Ref. 8) for all of the isospin-conserving reactions discussed. They are compared with the angular-distribution data in Fig. 8. In these calculations we have used neutron, proton, and excess-neutron nuclear densities resulting from Hartree-Fock calculations which used a Skyrme III force.[14] The DCX cross sections are sensitive to the details of these densities, especially near the nuclear surface. No second-order isoscalar (ρ^2), isovector ($\rho\Delta\rho$), or isotensor ($\Delta\rho^2$) terms have been included in these calculations. The failure of the angular-distribution calculations at $T_\pi=164$ MeV and the partial success of the calculations at $T_\pi=292$ MeV indicate the complexity of the DCX reaction mechanism near the Δ_{33} resonance energy and suggest the need for a second amplitude in the reaction.

The six angular distributions are plotted as a function of qR in Fig. 9, where q is the momentum transfer and R is a suitable strong absorption radius for the target nuclei.

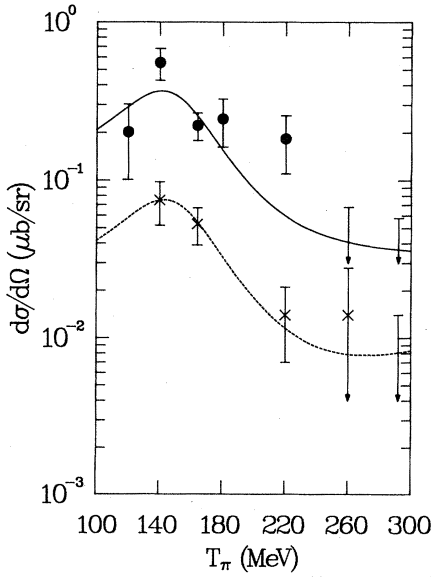

FIG. 7. Excitation functions for ^{14}C(π^+,π^-)^{14}O($E_x\simeq5.9$ MeV) (circles) and ^{56}Fe(π^+,π^-)^{56}Ni (g.s.) (crosses). The curves are obtained from a Breit-Wigner expression, plus a background term.

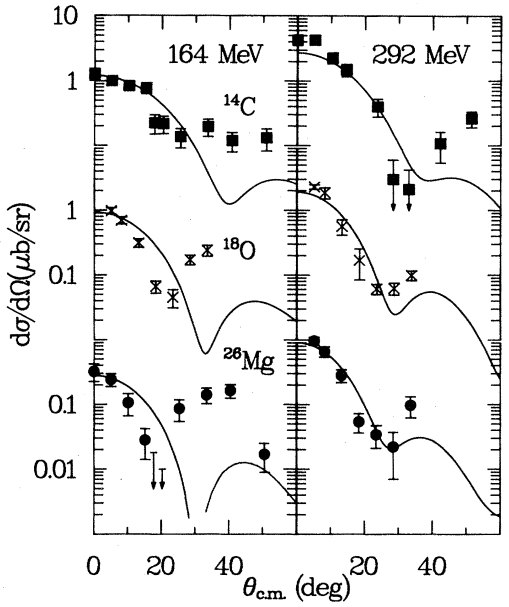

FIG. 8. Angular distributions at $T_\pi=164$ and 292 MeV for the reactions ^{14}C(π^+,π^-)^{14}O(DIAS) (squares), ^{18}O(π^+,π^-)^{18}Ne(DIAS) (crosses, from Ref. 1) and ^{26}Mg(π^+,π^-)^{26}Si(DIAS) (circles). The data for the latter at $T_\pi=292$ MeV are from Ref. 1. The curves are lowest order optical potential calculations from the theory of Ref. 8.

Values of R for ^{14}C, ^{18}O, and ^{26}Mg are 3.18, 3.46, and 3.91 fm, respectively, calculated from $R=1.32A^{1/3}$. At $T_\pi=164$ MeV, the angular distributions exhibit minima at $qR\simeq1.7$, whereas at $T_\pi=292$ MeV the minima appear at $qR\simeq3.5$.

The angular distribution for ^{14}C(π^+,π^-)^{14}O($E_x\simeq5.9$ MeV) is shown in Fig. 10. Poor statistics prevent us from making meaningful comparisons with the known characteristics of nonanalog DCX reactions, but the data are consistent with the presence of a minimum near 30°.

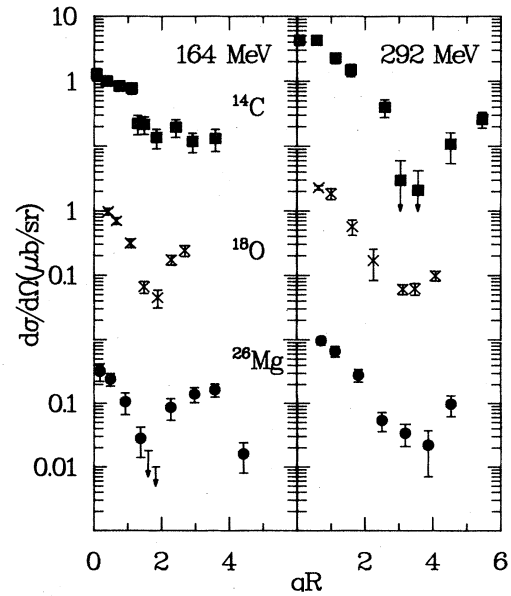

FIG. 9. The same data as in Fig. 6 plotted vs qR.

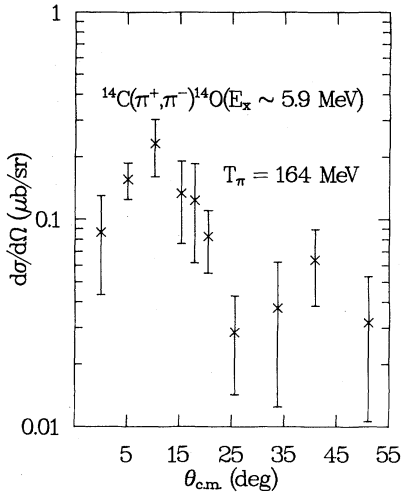

FIG. 10. Angular distribution for $^{14}C(\pi^+,\pi^-)^{14}O(E_x \simeq 5.9$ MeV).

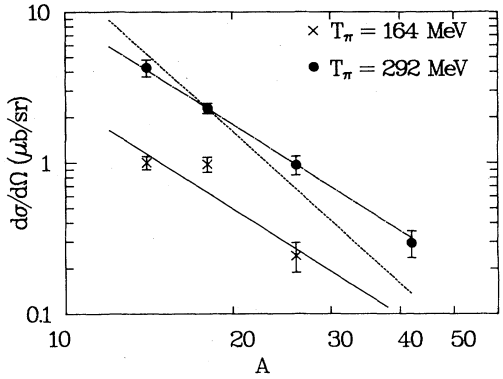

FIG. 11. Forward angle cross sections as a function of target mass for $T_\pi = 164$ and 292 MeV. ^{18}O was measured by Greene *et al.* (Ref. 1). ^{26}Mg at 292 MeV was measured by Greene *et al.*, ^{42}Ca is from Ref. 4, and ^{56}Fe is from Ref. 2. The dot-dash and solid lines are an $A^{-7/3}$ mass dependence at 292 and 164 MeV, respectively. The dashed line is an $A^{-10/3}$ mass dependence.

IV. DISCUSSION

Forward angle cross sections for transitions to double isobaric analog states as a function of target mass for $T=1$ target nuclei are shown in Fig. 11, with straight lines corresponding to an $(N-Z)(N-Z-1)A^{-7/3}$ mass dependence, and $(N-Z)(N-Z-1)A^{-10/3}$ for comparison. The $A^{-7/3}$ expression better describes the data at both energies and the agreement with the curve is better at 292 MeV than at 164 MeV. We know of no fundamental significance of this observed mass dependence; however, Johnson and Siciliano have shown that the geometric $(N-Z)(N-Z-1)A^{-10/3}$ dependence is violated when an isotensor term is included in the pion-nucleus optical potential.[8] The addition of ρ^2 dependent terms to the pion-nucleus optical potential can describe existing 164 MeV SCX and $T \geq 1$ DCX data for transitions to isobaric analog states.[9] But we note that when $T > 1$ data are included, the forward angle DCX data are fit better by $(N-Z)(N-Z-1)A^{-10/3}$.

A varying A dependence as a function of energy for the analog (π^+,π^0) 0° differential cross section has been noted by Sennhauser *et al.*[15] Based on fits to SCX data for $7 \leq A \leq 208$, the mass dependence changes from about $A^{-1.4}$ at $T_\pi = 100$ MeV to $A^{-1.1}$ at $T_\pi = 295$ MeV. There is no subset of analog DCX data for which this same trend is observed.

There are two types of excitation functions for analog DCX reactions: those for $A = 14$ and 56, which monotonically increase with pion energy, and which bracket the other type, as seen with $A = 18$, 26, and 42. In light of current DCX work, the $A = 14$ and 56 excitation functions may indicate negligible second-order effects, such as ρ^2 optical potential terms, or may point to the absence of competing nonanalog reaction mechanisms.[16–18] Conversely, the $A = 18$, 26, and 42 excitation functions indicate that at least one of these effects must be taken into account to explain the data.

The ^{14}C, ^{18}O, and ^{26}Mg angular distributions at $T_\pi = 164$ MeV possess minima at $qR \simeq 1.7$, while at 292 MeV the minima appear at $qR \simeq 3.5$, the latter consistent with first-order optical-potential calculations. As of now there are no angular distributions for ^{42}Ca and ^{56}Fe.

An accurate theoretical description of analog DCX may require understanding DCX on $T=0$ target nuclei, for which cross sections differ in energy, angular, and mass dependence from DCX on $T=1$ target nuclei. The parametrization of Johnson and Siciliano[8] of the second-order π-nucleus optical potential is only slightly A dependent, and it is just these parameters that fit the angular distributions for analog DCX.[9] Thus it appears that the $T=0$ measurements cannot be explained within this context. It remains to be seen if core-excitation effects can account for the observed energy dependence[5] for a variety of nuclei.

It has been speculated that DCX is sensitive to $\Delta_{3/2,3/2}(1232)$ presence in nuclear wave functions.[6,19] If it is necessary to invoke delta admixtures in the wave functions of these nuclei for DCX on $T=0$ targets, then the same must be done for analog transitions, since an approximate description of many of the $T=1$ nuclei studied (viz., ^{14}C, ^{18}O, ^{26}Mg, and ^{42}Ca) is a $T=0$ core coupled to two neutrons.

This work was supported in part by the Natural Sciences and Engineering Research Council of Canada, The Robert A. Welch Foundation, The National Science Foundation, and The Department of Energy.

*Present address: Los Alamos National Laboratory, Los Alamos, NM 87545.
†Present address: Indiana University, Bloomington, IN 47401.
‡Permanent address: University of Pennsylvania, Philadelphia, PA 19104.

[1] S. J. Greene, W. J. Braithwaite, D. B. Holtkamp, W. B. Cottingame, C. F. Moore, G. R. Burleson, G. S. Blanpied, A. J. Viescas, G. H. Daw, C. L. Morris, and H. A. Theissen, Phys.

Rev. C **25**, 927 (1982).

[2]P. A. Seidl, R. R. Kiziah, M. K. Brown, C. Fred Moore, C. L. Morris, H. Baer, S. J. Greene, G. R. Burleson, W. B. Cottingame, L. C. Bland, R. Gilman, and H. T. Fortune, Phys. Rev. Lett. **50**, 1106 (1983).

[3]M. B. Johnson, Phys. Rev. C **22**, 192 (1980).

[4]G. A. Miller, Phys. Rev. C **24**, 221 (1981).

[5]L. C. Bland, R. Gilman, M. Carchidi, K. Dhuga, C. L. Morris, H. T. Fortune, S. J. Greene, P. A. Seidl, and C. Fred Moore, Phys. Lett. **128B**, 157 (1983).

[6]C. L. Morris, H. T. Fortune, L. C. Bland, R. Gilman, S. J. Greene, W. B. Cottingame, D. B. Holtkamp, G. R. Burleson, and C. Fred Moore, Phys. Rev. C **25**, 3218 (1982).

[7]L. C. Liu, Phys. Rev. C **27**, 1611 (1983).

[8]M. B. Johnson and E. R. Siciliano, Phys. Rev. C **27**, 1647 (1983).

[9]S. J. Greene, C. J. Harvey, P. A. Seidl, R. Gilman, E. R. Siciliano, and M. B. Johnson (unpublished).

[10]Carol J. Harvey, Helmut W. Baer, J. A. Johnstone, C. L. Morris, S. J. Seestrom-Morris, D. Dehnhard, D. B. Holtkamp, and S. J. Greene, submitted to Phys. Rev. C.

[11]H. A. Theissen *et al.*, Los Alamos Scientific Laboratory Report No. LA-4534-MS, 1970 (unpublished); H. A. Theissen, J. C. Kallne, J. F. Amann, R. J. Peterson, S. J. Greene, S. L. Verbeck, G. R. Burleson, S. G. Iverson, A. W. Obst, K. K. Seth, C. F. Moore, J. E. Bolger, W. J. Braithwaite, D. C. Slater, and C. L. Morris, Los Alamos Scientific Laboratory Report No. LA-6663-MS, 1977; S. J. Greene, W. J. Braithwaite, D. B. Holtkamp, W. B. Cottingame, C. F. Moore, C. L. Morris, H. A. Theissen, G. R. Burleson, and G. S. Blanpied, Phys. Lett. **88B**, 62 (1979).

[12]G. Rowe, M. Salomon, and R. H. Landau, Phys. Rev. C **18**, 584 (1978).

[13]M. O. Kaletka, Ph.D. thesis, Northwestern University, 1983; Los Alamos National Laboratory Report No. LA-9947-T, 1984.

[14]M. Beiner, H. Flocard, Nguyen Van Giai, and P. Quentin, Nucl. Phys. **A238**, 29 (1975).

[15]U. Sennhauser, E. Piasetzky, H. W. Baer, J. D. Bowman, M. D. Cooper, H. S. Matis, H. J. Ziock, J. Alster, A. Erell, M. A. Moinester, and F. Irom, Phys. Rev. Lett. **51**, 1324 (1983).

[16]S. J. Greene, D. B. Holtkamp, W. B. Cottingame, C. Fred Moore, G. R. Burleson, C. L. Morris, H. A. Theissen, and H. T. Fortune, Phys. Rev. C **27**, 924 (1982).

[17]S. J. Greene, W. B. Cottingame, G. R. Burleson, L. C. Bland, R. Gilman, H. T. Fortune, C. L. Morris, D. B. Holtkamp, and C. Fred Moore, Phys. Rev. C **27**, 2375 (1983).

[18]R. Gilman, L. C. Bland, Peter A. Seidl, C. Fred Moore, C. L. Morris, Steven J. Greene, and H. T. Fortune, Nucl. Phys. (in press).

[19]L. C. Bland, H. T. Fortune, S. J. Greene, C. Fred Moore, and C. L. Morris, J. Phys. G **8**, L173 (1982); M. B. Johnson, E. R. Siciliano, H. Toki, and A. Wirzba, Phys. Rev. Lett. **52**, 593 (1984).